Drug specificity and affinity are encoded in the probability of cryptic pocket opening in myosin motor domains

Artur Meller[1,2], Jeffrey M. Lotthammer[1], Louis G. Smith[1], Borna Novak[1,2], Lindsey A. Lee[5,6], Catherine C. Kuhn[1], Lina Greenberg[1], Leslie A. Leinwand[5,6], Michael J. Greenberg[1], Gregory R. Bowman[4,1,3,‡]

1 Department of Biochemistry and Molecular Biophysics, Washington University in St. Louis, 660 S Euclid Ave, St. Louis, MO, 63110

2 Medical Scientist Train Program, Washington University in St. Louis, 660 S Euclid Ave., St. Louis, MO, 63110

3 Center for the Science and Engineering of Living Systems, Washington University in St. Louis, 1 Brookings Dr., St. Louis, MO, 63130

4 Department of Biochemistry and Biophysics, University of Pennsylvania, Philadelphia, PA, 19104

5 Molecular, Cellular, and Developmental Biology Department, University of Colorado Boulder, Boulder, CO, 80302

6 BioFrontiers Institute, Boulder, CO, 80302

‡ Corresponding author (grbowman@seas.upenn.edu)

Abstract

The design of compounds that can discriminate between closely related target proteins remains a central challenge in drug discovery. Specific therapeutics targeting the highly conserved myosin motor family are urgently needed as mutations in at least 6 of its members cause numerous diseases. Allosteric modulators, like the myosin-II inhibitor blebbistatin, are a promising means to achieve specificity. However, it remains unclear why blebbistatin inhibits myosin-II motors with different potencies given that it binds at a highly conserved pocket that is always closed in blebbistatin-free experimental structures. We hypothesized that the probability of pocket opening is an important determinant of the potency of compounds like blebbistatin. To test this hypothesis, we used Markov state models (MSMs) built from over 2 milliseconds of aggregate molecular dynamics simulations with explicit solvent. We find that blebbistatin's binding pocket readily opens in simulations of blebbistatin-sensitive myosin isoforms. Comparing these conformational ensembles reveals that the probability of pocket opening correctly identifies which isoforms are most sensitive to blebbistatin inhibition and that docking against MSMs quantitatively predicts blebbistatin binding affinities (R^2=0.82). To test our ability to make blind predictions, we predicted blebbistatin's binding affinity for an isoform (Myh7b) whose blebbistatin sensitivity was unknown. Encouragingly, we find good agreement between the predicted and measured IC50 (0.67 μM vs. 0.36 μM). Therefore, we expect this framework to be useful for the development of novel specific drugs across numerous protein targets.

Significance

Drug development requires the discovery of compounds which specifically target one member of a protein family without triggering side effects that arise from interactions with other related proteins. Myosins are a family of motor proteins that are drug targets for heart diseases, cancer, and parasitic infections. Here, we investigate why the compound blebbistatin specifically inhibits some myosins more potently than others, even though its binding site is closed in all known experimental structures. We find that the blebbistatin binding pocket opens in molecular dynamics simulations of certain myosin motors, and that the probability of opening predicts how potently blebbistatin inhibits a particular motor. Our work suggests that differences in cryptic pocket formation can be exploited to develop specific therapeutics.

Introduction

Achieving specificity is a major challenge in the design of novel drugs. An effective drug must bind its target protein tightly and avoid triggering unwanted side effects that might arise due to off-target interactions with other proteins. This problem is especially challenging when targeting specific members of protein families when multiple closely related isoforms with similar structures are expressed. Another notoriously difficult problem is targeting enzymes with substrates, such as ATP, that are shared across many protein families [1], because compounds that compete with endogenous ligands at active sites may trigger off-target effects.

Targeting allosteric sites offers several practical advantages for drug design. Unlike drugs targeting active sites, allosteric compounds can enhance desirable protein functions, in addition to the more classic drug design strategy of inhibiting undesirable activities.[2] Allosteric sites are often less conserved than active sites[3], making it easier to achieve specificity. Indeed, several highly specific allosteric compounds have been serendipitously discovered through high-throughput screens. These allosteric compounds target diverse proteins, such as G-protein-coupled receptors[4], myosins[5], kinases[6], and β-lactamases[7]. Despite these successes, *de novo*, structure-based, rational drug design efforts targeting allosteric sites are difficult because most experimental structural studies only offer a limited snapshot of a protein's larger conformational landscape. In solution, proteins occupy a diverse set of conformational states, and some allosteric binding sites are not readily apparent from these static structures.[8] Discovering and targeting such "cryptic" pockets may be an appealing strategy for achieving specificity towards clinically relevant proteins deemed 'undruggable' by conventional structural studies.[9]

Myosins are a ubiquitous superfamily of ATPases that hold potential as drug targets for numerous diseases. Myosins are responsible for many cellular processes including endocytosis,

cell division, muscle contraction, and long-range transport.[10] Compounds targeting a subset of striated muscle myosins have been developed and shown great promise in clinical trials for heart failure[11] and hypertrophic cardiomyopathy[12]. Recently, the myosin inhibitor, mavacamten, received FDA approval for the treatment of symptomatic obstructive hypertrophic cardiomyopathy.[13] Despite this progress, there is a need for additional myosin modulators in the settings of heart and skeletal muscle diseases[14,15], cancer[16], and parasitic infections[17]. However, targeting specific myosin isoforms remains extremely difficult because there are 38 myosin genes in the human genome with the typical cell in the human body expressing several myosin isoforms.[18] Furthermore, myosins with divergent cellular roles and biochemical properties share a highly conserved motor domain fold and active site structure.[19] High-throughput screens have revealed a handful of promising small molecules that allosterically inhibit or activate myosins with varying degrees of specificity.[20] Developing a quantitative understanding of how these allosteric modulators achieve specificity would improve our ability to design novel therapeutics targeting specific myosin isoforms.

Blebbistatin is a myosin-II specific allosteric inhibitor which can be used to understand the molecular mechanisms governing specificity. Blebbistatin was discovered in a high-throughput screen targeting nonmuscle myosin IIs.[21] However, further experiments revealed that blebbistatin broadly inhibits other myosins-II isoforms, such as fast skeletal, β-cardiac, and smooth muscle myosin with varying IC50s, but not other myosin families, such as myosin-Xs and myosin-Vs.[22] Blebbistatin inhibits myosin ATPase by preventing the release of phosphate from the active site; however, experimental structures of blebbistatin bound to myosin reveal that it binds in a cleft approximately 9 Å from the active site, consistent with its designation as an allosteric effector.[23]

The mechanism of blebbistatin's specificity is not completely understood. Previous studies have posited that blebbistatin specifically inhibits myosin-IIs because of a single residue difference between myosin-IIs and other myosins at the blebbistatin binding site (Fig. 1B, Fig. 1D).[24] However, it is much less clear what the molecular determinants of blebbistatin specificity are within the myosin-II family. For example, across multiple experiments[22,25–29], smooth muscle myosin is inhibited less potently than nonmuscle myosin IIA, despite perfect sequence identity between the residues that line the blebbistatin-binding pocket in these two isoforms (Fig. 1B, Table S1). It has previously been suggested that blebbistatin binds at a "cryptic" pocket that is usually closed in crystal structures of myosins without a bound blebbistatin.[8] Indeed, the blebbistatin binding site is closed in crystal structures of two blebbistatin-sensitive myosin isoforms (Fig. 1C). These results suggest that blebbistatin's specificity is also encoded by factors beyond the sequence of the binding pocket.

We hypothesized that blebbistatin potency among myosin-II family members is encoded in the ensemble of structures that myosins adopt in solution, with more sensitive isoforms (i.e., lower IC50s) having a higher probability of adopting conformations with an open blebbistatin-binding pocket. A growing body of work has strengthened the view that cryptic pockets closed in crystal structures can open in excited structural states explored in solution.[30–34] Hence, we reasoned that the blebbistatin cryptic pocket would open in all-atom molecular dynamics simulations. To test our hypothesis and identify the molecular determinants of blebbistatin specificity in myosin motors, we leverage all-atom molecular dynamics simulations, Markov State Models (MSMs), and a novel MSM-based approach to aggregating docking results across structural ensembles for accurate prediction of binding affinities.

Results

Blebbistatin's cryptic binding pocket opens in simulations

We first sought to establish whether the blebbistatin pocket is open in any blebbistatin-free myosin experimental structures or if it is a "cryptic" site. Cryptic pockets are cavities that open and close as a protein fluctuates in solution but are typically closed and therefore hidden in experimental structures.

To assess whether the blebbistatin-binding site is cryptic, we queried the Protein Data Bank (PDB) for an exhaustive set of myosin motor domains, yielding 124 structures that were not crystallized with blebbistatin or blebbistatin derivatives (see Methods). We then assessed the degree of pocket opening at the blebbistatin binding site using the LIGSITE pocket detection algorithm[35]. Briefly, LIGSITE finds concavities on a protein surface by identifying grid points that are surrounded by protein but not in contact with protein atoms (see Methods). Those LIGSITE grid points that were within 5 Å of an aligned blebbistatin molecule were considered part of the blebbistatin pocket. The pocket was considered open if its volume matched or exceeded that of the *holo*, or ligand-bound, structure.

We find that all known blebbistatin-free experimental structures of the myosin motor domain have a closed blebbistatin pocket (Fig. 2A). Not a single blebbistatin-free experimental structure reaches the *holo* pocket volume, and the majority of *apo* structures have less than half of the *holo* pocket volume. In *apo* myosin experimental structures, a leucine residue in the U50 linker[23], a highly conserved loop in the upper 50-kDa domain, always points into the blebbistatin pocket, creating a steric impediment to binding (Fig. 2A inset). While the blebbistatin binding site has previously been annotated as a cryptic pocket, previous analyses were restricted to a subset of *apo* myosin experimental structures that matched the *holo* structure's sequence exactly.[8] Here,

we have shown that all available blebbistatin-free experimental structures of the myosin family lack an open blebbistatin pocket.

Even if the blebbistatin pocket is absent in *apo* experimental structures, we reasoned that the pocket might open in excited states accessible in all-atom molecular dynamics (MD) simulations. Recent work demonstrates that in solution myosins sample a broad range of conformations driven by thermal fluctuations[36,37], even though all myosin motor domains share a common fold.[19] To assess whether the blebbistatin pocket opens in solution without blebbistatin present, we used molecular dynamics to simulate the motor domain of human fast skeletal myosin IIA (*MYH2*). Fast skeletal myosin is potently inhibited by blebbistatin (average IC50: 0.3 μM[22,28,38]), so we hypothesized that its blebbistatin pocket would open extensively in simulation.

We constructed Markov State Models (MSMs) from over 80 microseconds (Table S2) of simulations of the actin-free, ADP-phosphate-bound fast skeletal myosin motor domain. MSMs of molecular simulations are network models of free energy landscapes composed of many conformational states and the probabilities of transitioning between these states.[39] We constructed MSMs of the conformations seen in the blebbistatin pocket by clustering structures in a kinetically relevant projection of backbone and sidechain dihedral angles (see Methods). To measure blebbistatin pocket opening, we measured pocket volumes at the blebbistatin binding site using the LIGSITE algorithm as described above. We then quantified the probability of pocket opening based on the probability of each structure in the MSM (see Methods).

In contrast to myosin crystal structures, we find that simulations reveal extensive opening of the blebbistatin pocket. The distribution of pocket volumes from simulation is substantially right-shifted relative to the distribution seen in crystal structures (Fig. 2B). Even though our simulations were started from a closed *apo* conformation, all 8 long (>500 nanosecond)

independent simulations of fast skeletal myosin II exceed the volume seen in the *holo* crystal structure (Fig. S1). Indeed, the blebbistatin pocket is open in about one-third of conformations at equilibrium (p_{open}=0.31). When we visually inspected structures from simulation that had reached the *holo* pocket volume (Fig. 2C), we find that the blebbistatin pocket geometry closely matches that of the *holo* crystal structure (the root mean square deviation for the structure depicted in Fig. 2C was 0.55 Å when considering the backbone heavy atom and Cβ positions of residues in contact with blebbistatin). While the leucine (L270 in skeletal muscle myosin) in the U50 linker always points into the blebbistatin pocket in crystal structures, this leucine residue rotates toward its *holo* position, creating a pocket where blebbistatin can bind (Fig. 2C). Thus, we find that *apo* simulations can capture blebbistatin cryptic pocket opening that is not seen in myosin crystal structures and that MSMs can be used to quantify the probability of blebbistatin pocket opening.

Blebbistatin's cryptic pocket preferentially opens in the ADP*Pi state

Given that blebbistatin's cryptic pocket opens in simulation, we wondered if pocket opening was dependent on the nucleotide present in the myosin active site. Biochemical experiments have shown that blebbistatin binds to rabbit fast skeletal muscle myosin with ~10-fold greater affinity when myosin is bound to ADP and phosphate instead of ATP [40]. Hence, we hypothesized that blebbistatin pocket opening would be more likely in simulations of myosin bound to ADP*Pi than it would be in simulation of myosin bound to ATP.

To test this hypothesis, we ran long simulations of human fast skeletal muscle myosin IIA (*MYH2*) from a homology model of a post-rigor crystal structure with ATP in its active site (PDB ID: 6FSA) [41] and assessed opening with LIGSITE as described above. We then quantified

the probability of blebbistatin pocket opening in a MSM of the blebbistatin pocket in the ATP-bound state.

We find that while blebbistatin pocket opening occurs in both nucleotide states, it is substantially more probable in simulations of the ADP*Pi state than in the ATP state (Fig. 3A). In the ADP*Pi state, the equilibrium probability of blebbistatin pocket opening is 0.31. In the ATP state, it is only 0.08 (Fig. 3B). This finding is consistent with the experimental results showing that blebbistatin is more likely to bind to a myosin bound to ADP and phosphate, trapping it in this state of the mechanochemical cycle[42]. Furthermore, this dependence between the nucleotide state in the active site and blebbistatin pocket opening indicates that simulations are capturing the allosteric coupling between these two parts of the myosin molecule.

The probability of cryptic pocket opening predicts trends in blebbistatin potency

We reasoned that an important determinant of how potently blebbistatin inhibits a myosin isoform is how likely the blebbistatin pocket opens. If pocket opening is more likely in one isoform, then stabilizing the open state should be easier than in an isoform where pocket opening is less probable. Thus, we hypothesized that the blebbistatin pocket would be more likely to open in myosin isoforms more potently inhibited by blebbistatin (i.e., those with lower IC50s).

We first assessed whether pocket opening probabilities could distinguish blebbistatin-sensitive isoforms (IC50 < 150 μM) from blebbistatin-insensitive isoforms (IC50 > 150 μM). To compare sensitive and insensitive isoforms, we calculated pocket volumes at the blebbistatin binding site in an existing dataset of *apo* myosin motor equilibrium fluctuations.[36] While blebbistatin binds with reduced affinity to nucleotide-free myosins like the ones in these simulations[40], our previous work demonstrated that simulations can capture pocket opening in

excited states even in the absence of relevant binding partners. We utilized the LIGSITE pocket detection algorithm to assign a blebbistatin pocket volume to each state in the myosin motor MSMs following the same procedure as described above. We then defined compatible states as those conformations where the blebbistatin pocket volume reached or exceeded its volume in a blebbistatin-bound crystal structure of *D.d*. myosin-II (PDB: 1YV3).[23]

We find that the probability of adopting a pocket conformation compatible with blebbistatin binding is higher among myosin-II isoforms compared to other isoforms. We observe large differences in the blebbistatin pocket volume distributions between MSMs of myosin-IIs and non-myosin-IIs (Fig. 4). In simulations of unconventional myosin-V and myosin-Ib, the blebbistatin pocket stays entirely closed despite almost 300 microseconds of aggregate simulation time per isoform. In contrast, all myosin-IIs sample conformations with pocket volumes that exceed the *holo* pocket volume. Interestingly, among myosin-IIs the probability of pocket opening (smooth muscle myosin < nonmuscle myosin IIb < β-cardiac myosin) correctly predicts the rank order of IC50 values (Fig. S3).

Thus, blebbistatin pocket opening differs between divergent myosin isoforms when there are large sequence differences at the binding site. While myosin-IIs contain small sidechains at the A466 position (skeletal muscle myosin numbering), other myosin families contain aromatic sidechains which point into the pocket, reducing the pocket volume available for blebbistatin binding (Fig. 1B, 1D). Moreover, while myosin-II isoforms have a conserved pocket that opens during simulations of nucleotide-free motor domains, the probability of opening appears to correlate with blebbistatin's potency.

To relate the probability of pocket opening more precisely to blebbistatin potency, we ran simulations of several sensitive myosin-II isoforms (β-cardiac myosin, nonmuscle myosin IIA,

and smooth muscle myosin) that exhibit a broad range of blebbistatin IC50 values (Fig 1B). Since blebbistatin preferentially inhibits myosin when the motor domain is bound to ADP and phosphate[40], we ran these MD simulations with ADP*Pi in the active site. Each of the myosin-II isoforms was launched from a closed, blebbistatin-free starting conformation (Fig. 5A). We observed pocket opening in all simulations of myosin-II isoforms, but the likelihood of opening was substantially enhanced in simulations of fast skeletal muscle myosin II and β-cardiac myosin. Indeed, in simulations of both skeletal muscle myosin II and β-cardiac myosin, a rolling average (window of 10 ns) of pocket volumes exceeds the *holo* volume for over 500 ns while in simulations of nonmuscle myosin IIA and smooth muscle myosin the pocket only opens transiently a handful of times (Fig. 5, S2).

We find that the probability of pocket opening is larger for myosin-II isoforms more potently inhibited by blebbistatin. To quantify probabilities of pocket opening, we constructed a MSM of the conformations seen in the blebbistatin pocket for each isoform separately. We then computed the blebbistatin pocket volume for all structures visited by the simulations, assigned a probability to each structure based on the MSM, and found the overall probability of reaching a pocket volume matching or exceeding that of a *holo* crystal structure (see Methods). Among myosin-IIs, the probability of pocket opening is substantially higher for fast skeletal myosin IIA and β-cardiac myosin than it is for nonmuscle myosin IIA and smooth muscle myosin (Fig. 5E). Smooth muscle myosin has the lowest probability of pocket opening (~0.0005), so its free energy difference between open and closed states is the largest. Similarly, nonmuscle myosin IIA has a slightly larger but still low probability of pocket opening (~0.001), consistent with its intermediate IC50. Conversely, both fast skeletal myosin IIA (p_{open}=0.31) and β-cardiac myosin (p_{open}=0.46) have large probabilities of adopting open states in their MSMs. Given that β-cardiac

myosin has a higher opening probability but is less sensitive to blebbistatin, we wondered if volume is a useful, yet incomplete descriptor, for assessing specificity. To test this hypothesis, we turned to molecular docking to see if we could quantitatively predict the binding affinity for blebbistatin between these myosin-II isoforms by using ensembles of structures from our simulations.

MSM-docking quantitatively predicts blebbistatin's potency

We reasoned that molecular docking could improve our ability to predict blebbistatin's potency by considering the chemical environment of the pocket rather than just the volume available to it. Some of the states we had labeled as closed based on pocket volume, especially those with volumes slightly less than the *holo* structure, might be able to accommodate blebbistatin in alternate poses. In contrast, some open states may be less compatible with binding than others. We have previously shown that docking compounds to a diverse set of conformations from a Markov State Model improves agreement with experiment.[43] In this work, we wished to dock to open and closed structures from the ensemble to generate a robust estimate of the free energy of blebbistatin binding.

To determine whether crystal structures were sufficient to explain differences in blebbistatin potency, we first docked blebbistatin to single open and closed structures found in the PDB. When we docked to the closed *apo* experimental structures from which simulations were launched, we unsurprisingly found very poor docking scores for all myosin-II isoforms (Fig. S6). There were no subtle structural differences between experimental structures or adjacent pockets that might explain variation in blebbistatin potency. We also docked blebbistatin to homology models of the 4 different myosin-IIs considered above in the *holo* crystal structure. This allowed

us to interrogate if a single binding-competent structure with the appropriate pocket residues could explain blebbistatin's specificity. We found virtually no differences in predicted binding affinities between myosin-IIs using docking to these static structures (Fig. S6).

Next, we docked blebbistatin to the ensemble of structures represented in our MSMs. Specifically, we used AutoDock Vina to dock blebbistatin against representative structures from each state of our MSM within a box centered on the blebbistatin binding site (see Methods). After completing docking, we investigated both the highest scoring poses and those poses with the lowest blebbistatin RMSD from *holo*. Encouragingly, the highest scoring pose for skeletal muscle myosin and β-cardiac myosin is very similar to blebbistatin's pose in the previously determined experimental *holo* crystal structure (RMSD < 3 Å for the ligand heavy atoms, Fig. S8). All four myosin-II isoforms had structures with ligand heavy atom RMSD < 3 Å from the *holo* pose, but the conformational ensembles of skeletal muscle and β-cardiac myosin are substantially enriched for such structures (Fig. S7).

We find that computationally predicted blebbistatin binding free energies based on state populations from our Markov State Models closely match experimental values. To calculate a blebbistatin binding free energy for each isoform, we assigned a probability to each structure from docking based on the overall probability of that structure's MSM state and the number of other structures that were mapped to that MSM state (see Methods). Finally, we aggregated the docking results by finding a weighted average of binding constants and converting this value to a free energy of binding. To assess the accuracy of these predictions, we pooled IC50 measurements from all available experiments and converted these measurements to binding free energies under the assumption that IC50 was essentially equivalent to K_i (see Methods for detailed rationale). When we compared the predicted binding affinity of blebbistatin from

docking to experimental averages, we find that these parameters are well correlated (Fig. 6A, R^2=0.82). Moreover, we note that the absolute value of our predictions of binding free energy are in good agreement with binding affinities estimated from experiment (root mean square error of 0.7 kcal/mol). Thus, our results suggest that docking to the ensemble of structures with MSM weighting provides an efficient way to rapidly assess the relative binding affinity of a compound within the same protein family.

To test our ability to make blind predictions with this approach, we computationally and experimentally interrogated blebbistatin inhibition of a sarcomeric myosin-II isoform called Myh7b whose sensitivity to blebbistatin had not been determined. Myh7b's blebbistatin binding site is identical to β-cardiac myosin's. However, there are numerous sequence differences immediately surrounding blebbistatin's binding site (7 positions that differ between Myh7b and β-cardiac myosin within 1 nm of blebbistatin's binding site). In simulations of a homology model of its motor domain, Myh7b had substantial pocket opening (Fig. S10). Moreover, when we docked to representative structures from the Myh7b simulations and aggregated predicted binding affinities using its MSM, we predict that the binding affinity of blebbistatin for Myh7b is -8.8 kcal/mol. Thus, we hypothesized that Myh7b would be highly sensitive to blebbistatin inhibition and that its IC50 would be more similar to the IC50 of fast skeletal and β-cardiac myosin than that of smooth muscle myosin.

We find that blebbistatin potently inhibits the actin-activated ATPase activity of Myh7b (Fig. 6B, IC50: 0.36 μM). We used recombinant human Myh7b and β-cardiac myosin S1 constructs expressed in C_2C_{12} cells in our experiments. We measured NADH-linked ATPase rates at increasing concentrations of blebbistatin (0.3125 μM to 20 μM) and fit a hyperbolic Hill equation to the data to determine the IC50. As a control, we measured the IC50 value for β-

cardiac myosin S1. We obtain an IC50 of 1.12 ± 0.29 μM (error indicates standard deviation between replicates), a value which closely matches with previously published IC50s (Fig. S11). Consistent with our hypothesis and the computational prediction of blebbistatin's affinity for Myh7b based on MSM-docking (0.67 μM), we obtain an experimentally measured IC50 for Myh7b (0.36 ± 0.08 μM) that is more similar to fast skeletal and β-cardiac myosin's IC50 than smooth muscle myosin's IC50. Thus, our experiments provide additional validation for the MSM-docking approach.

Discussion

A ligand's specificity is most typically attributed to differences in the composition of residues at the ligand binding site. Sequence variation at a binding site can modify the shape of a binding pocket or alter the types of interatomic interactions formed between a ligand and its target protein. Mutagenesis experiments have shown that sequence differences in the blebbistatin pocket are an important determinant of blebbistatin's selectivity for myosin-IIs.[27] While myosin isoforms outside the myosin-II family have a bulky aromatic residue that points into the blebbistatin pocket, myosin-IIs have smaller residues at that analogous position (Fig. 1D). However, the binding pocket residues that coordinate binding of blebbistatin are insufficient to fully explain its isoform specificity.

Our results highlight that the distribution of structural states explored in solution is an essential determinant of specificity. We find that differences in blebbistatin pocket dynamics are important determinants of differences in IC50 between myosin-II isoforms. Pocket opening is substantially more probable in skeletal muscle myosin than it is in smooth muscle myosin, consistent with blebbistatin's more potent effects on skeletal muscle myosin. Furthermore, even when the blebbistatin binding site is perfectly conserved between isoforms, such as in the cases of nonmuscle myosin-IIA and smooth muscle myosin, MSM-weighted docking predicts differences in blebbistatin affinity which are consistent with experimentally measured differences in IC50. Thus, pocket dynamics, together with differences in the blebbistatin pocket's residue composition are both important determinants of specificity.

Our findings agree with other studies that demonstrate the importance of pocket dynamics in modulating ligand specificity. Another myosin inhibitor, CK-571, which specifically targets smooth muscle myosin binds at a perfectly conserved binding site, suggesting an important role

for structural dynamics.[44] Furthermore, the CK-571 pocket has not been observed in ligand-free myosin structures. Similar results have been found in other systems. Positive allosteric modulators of a G-protein-coupled receptor bind at a dynamic cryptic pocket[34], and their selectivity has been attributed to differences in cryptic pocket opening. Together, a growing body of evidence suggests that cryptic pockets can be exploited to develop isoform-specific drugs against proteins with nearly identical crystal structures.

Finally, our results highlight the general capacity of computational modeling to capture how subtle sequence differences induce conformational preferences, which, in turn, can control function. Simulations that reveal how sequence variation impacts conformational dynamics have potential to bolster our understanding of how patient-specific mutations contribute to protein dysfunction and drug response as well as to guide the development of new therapeutics. Indeed, certain myosin variants associated with disease may show mutation-induced changes in dynamics that could be targeted as part of a precision medicine approach.[45,46] Thus, our work represents an important advancement towards physics-based precision medicine.

Methods

Structural bioinformatics

We queried the PDB for all experimental structures of myosin motor domains with a sequence identity cutoff of 10% to *hs MYH7*, resolution <= 4.0 Å, and a BLAST E-value less than 0.1. All PDBs satisfying these criteria were downloaded for further analysis. Some of these PDB files contained fragments of motor domains; therefore, the resulting database of PDBs was parsed further by selecting the largest chain in each crystal structure if the sequence was > 600 amino acids. A multiple sequence alignment was performed with 1YV3 as reference. Structures containing blebbistatin, or blebbistatin derivatives, were also excluded from the set (PDB: 6Z7U, 6YSY, 3MJX, 3BZ8,3BZ7, 3BZ9, 1YV3, 3MYK, 3MYH). The resulting alignment was used to identify ligand binding site for the blebbistatin binding pocket and pocket volumes were calculated on each of these structures with the LIGSITE pocket detection algorithm[35] with a minimum rank of 6, probe radius of 0.07 nm, and a minimum cluster size of 3 grid points.

Preparation of homology models

Initial structural models for each myosin isoform were generated with SWISS-MODEL.[47] Crystal structures for simulations were selected based on their sequence similarity to the isoform of interest. Higher resolution structures were prioritized. For 5N6A, the converter and N-terminal regions of the protein were replaced with the corresponding converter and N-terminal regions from 5N69 because these regions were poorly resolved in 5N6A. Below, the UniprotID of the respective human myosin isoform are provided as well as the relevant crystal structures used for modeling.

Isoform	Gene	UniprotID	Template Structure	Structural State
Fast Skeletal	MYH2	Q9UKX2	5N6A	PPS
β-Cardiac	MYH7	P12883	5N6A	PPS
Nonmuscle IIA	MYH9	P35579	5I4E	PPS
Smooth	MYH11	P35749	1BR2	PPS
MYH7b	MYH7B	A7E2Y1	5N6A	PPS
Fast Skeletal	MYH2	P12883	6FSA	PR

PPS indicates prepowerstroke while PR indicates post rigor.

Molecular dynamics simulations

GROMACS[48] was used to prepare and to simulate all proteins using the CHARMM36m force fields[49]. The protein structure was solvated in a dodecahedral box of TIP3P water[50] that extended 1 nm beyond the protein in every dimension. Thereafter, sodium and chloride ions were added to the system to maintain charge neutrality and 0.1 M NaCl concentration. Each system was minimized using steepest descent until the maximum force on any atom decreased below 1000 kJ/(mol x nm). The system was then equilibrated with all atoms restrained in place at 300 K maintained by the Bussi-Parinello thermostat[51] and the Parrinello-Rahman barostat[52].

Production simulations were performed in the CHARMM36m forcefield. Simulations were run in the NPT ensemble at 310 K using the leapfrog integrator, Bussi-Parinello thermostat, and the Parrinello-Rahman barostat. A 12 Å cutoff distance was utilized with a force-based switching

function starting at 10 Å. Periodic boundary conditions and the PME method were utilized to calculate the long-range electrostatic interactions with a grid density greater than 1.2 $Å^3$. Hydrogen bonds were constrained with the LINCS algorithm[53] to enable the use of a constant integration timestep of 2 fs.

Molecular dynamics simulations were initially performed in parallel from single starting structures first on our in-house supercomputing cluster or on Oracle Cloud Infrastructure using a combination of Tesla P100, Quadro RTX 6000, and NVIDIA RTX A5000 nodes. Five starting structures were obtained from RMSD clustering this initial trajectory data based on the pocket backbone and C-β positions. These starting structures were then used for additional simulations on Folding@home[54] (750 clones initiated with different velocities for each starting structure).

Markov State Models

To construct a Markov State Model[39] of the blebbistatin pocket, we first defined a subset of features that were relevant to blebbistatin pocket opening. We used backbone (phi, psi) and sidechain dihedrals of residues within 5 Å of the blebbistatin molecule as an input set of features describing the blebbistatin pocket.

To perform clustering in a kinetically relevant space, we applied time-structure-independent component analysis (tICA) to these features.[55] Specifically, we used a tICA lag time of 10 ns and retained the top n tICs for each isoform that accounted for 90% of kinetic variance using commute mapping.

To determine the number of microstates in our Markov State Model, we used a cross-validation scheme where trajectories were partitioned into training and testing sets.[56] Clustering into *k* microstates was performed using only the training set, and the test set trajectories were assigned to these *k* microstates based on the their Euclidean proximity in tICA space to each microstate's centroid. Using the test set only, an MSM was fit using maximum likelihood estimation (MLE)[57] and the quality of the MSM was assessed with the rank-10 VAMP-2 score of the transition matrix.[58]

Finally, Markov state models of the blebbistatin pocket were fit for each isoform separately using MLE. Lag times were chosen by the logarithmic convergence of the implied timescales test.[59] MSM construction was performed using the PyEMMA software package.[60]

Pocket Analysis

We calculated pocket volumes for the blebbistatin pocket using the LIGSITE algorithm.[35] Specifically, we used the LIGSITE implementation in the enspara software package[61] with a minimum rank of 6, probe radius of 0.07, and a minimum cluster size of 3 grid points. After generating pocket grid points for a myosin structure, we filtered those grid points in the blebbistatin pocket if they were within 2.5 Å of an aligned blebbistatin molecule. We employed a local alignment using homologous residues within 5 Å of blebbistatin. Finally, we required that pockets be continuous and selected the largest cluster of grid points defined as having a shortest inter-grid point distance of 1.5 Å.

To generate distributions of pocket volumes, we followed two different procedures. For the previously published dataset[36], we calculated volumes for each representative structure in the Markov State Model and weighted by the equilibrium probability of each state in the MSM. This was done because a) the size of the dataset prohibited calculating pockets for all simulation frames and b) these MSMs contained thousands of states and hence were likely to capture a substantial degree of heterogeneity in the blebbistatin pocket. For the new simulations generated for this work, we calculated pocket volumes for every structure we saved from our simulations (save rate of one frame per 20 ps) and then weighted each of these volumes by the probability of a given structure in that isoform's MSM, specifically the equilibrium probability of the MSM state that the structure is assigned to divided by the number of structures assigned to that MSM state. This second approach allows us to track the temporal evolution of pocket volumes in individual trajectories.

Docking

Docking against individual structures was performed using smina.[62,63] For each MSM state, we randomly extracted either 3 different structures from that state or $\pi_i * 2000$ different structures if that number exceeded 3/2000 (where $\pi_i$is the equilibrium probability of the MSM state). PDB files were converted to PDBQT files using AutoDockFR (ADFR suite). The ligand PDBQT files were generated using the same ADFR suite. The ligand charges were assigned using antechamber. To center the docking grid box on the blebbistatin binding pocket, we first selected backbone heavy atoms from residues within 0.5 nm of blebbistatin in its *holo* structure (PDB: 1YV3) and aligned this selection using an iterative procedure described in Grossfield et al.[64] We then used the centroid of the average structure from the final alignment as the center of our box— (0,0,0) in that coordinate system. All alignment and frame selection was done using LOOS.[65,66] For the docking search, we set the exhaustiveness was set to 8 and used the smina scoring function. Jug[67] was used to parallelize docking while gnu parallel[68] was used to parallelize receptor parameterization.

The overall free energy of binding from docking to an MSM can be written as:

$$\Delta G_{total} = -k_B T ln\left(\sum_i \pi_i K_{eqi}\right)$$

where $\pi_i$is the equilibrium probability of the MSM state and K_{eqi} is the equilibrium constant calculated from the docking score to that MSM state. Since the scoring function returns docking scores in kcal/mol, it is straightforward to convert to K_{eqi}.

Because we docked to multiple structures for each MSM state, we found a consensus docking score by using the following equation:

$$\Delta G_{total} = -k_B T ln\left(\sum_f \frac{\pi_{s_f}}{N_{s_f}} K_{eqi}\right)$$

where f is a structure from simulation, s is the MSM state that structure belongs to, N is the number of structures from that MSM state for which docking was performed, and pi is the equilibrium probability of that MSM state.

Protein Expression and Purification

Recombinant myosin was produced as previously described[69–71] with minor changes. Adenoviruses encoding human β-MyHC S1 (amino acids 1-842) and human MYH7b S1 (amino acids 1-850) followed by a flexible GSG linker and C-terminal PDZ binding peptide (RGSIDTWV) were used to infect differentiated C_2C_{12} cells. C_2C_{12} cells were harvested 4 days after infection, flash frozen in liquid nitrogen, and stored at -80 °C. Cell pellets were thawed and lysed using dounce homogenization in 50 mM Tris pH 8.0, 200 mM NaCl, 4 mM $MgCl_2$, 0.5% Tween-20, 5 mM DTT, 1 mM ATP, 0.2 mM PMSF, and 1X protease inhibitor cocktail (Millipore Sigma/Roche, 11873580001). Lysates were clarified by centrifugation at 39,000 x g for 25 minutes at 4 °C. The supernatant was filtered through 5 μM and 1.2 μM filters and applied to a column containing SulfoLink resin (ThermoFisher, 20402) coupled to PDZ. The column was washed with 30 mM Tris pH 7.5, 50 mM KCl, 5 mM $MgCl_2$, 1 mM DTT, and 1 mM ATP and myosin S1 (bound by endogenous C_2C_{12} light chains) was eluted using a peptide with tighter affinity for PDZ (WQTWV). Proteins were dialyzed against a storage buffer containing 20 mM MOPS pH 7.0, 25 mM KCl, 5 mM $MgCl_2$ and 10% sucrose, flash frozen in liquid nitrogen, and stored at -80 °C.

Actin was purified from porcine ventricles as previously described[72,73]. The concentration of actin was determined spectroscopically as previously described[72,73].

NADH-linked ATPase Measurements

Actin-activated ATPase rates were measured across a range of blebbistatin concentrations using the NADH-coupled assay in a 96-well plate[74] with a 0.1 μM myosin S1 concentration and 10 μM actin concentration. Before the experiment, actin was polymerized by dialysis in ATPase buffer containing 20 mM Imidazole, 10 mM KCl, 2mM $MgCl_2$, and 1 mM DTT followed by 1.1x molar ratio phalloidin stabilization. Experiments were conducted in ATPase buffer with the addition of the NADH-coupled enzymes (0.5 mM phospho(enol)pyruvate (Sigma, P0564), 0.47 mM NADH (Sigma, N7410), 100 U/mL pyruvate kinase (Sigma, P9136), and 20 U/mL lactate dehydrogenase (Sigma, L1254)). Blebbistatin (Selleckchem, S7099) was dissolved in DMSO. The blebbistatin concentration was varied using serial dilutions. Before gathering data, 2 mM ATP was added to each well. Experiments were performed at 25° C using a BioTek Syngergy H1 microplate reader. Absorbance was monitored at 340 nm and it decreased linearly with time. Rates for each well were determined based on the linear fitting of the absorbance as a function of time. A control well containing actin, no myosin, and 20 μM blebbistatin was used as a baseline. Finally, a Hill equation was fit to the data to determine an IC50 for each experiment. Each data point consists of 5 technical replicates.

Statistical Analysis

Bootstrapping was performed to generate error bars for each of the reported simulation measurements. Specifically, we performed 250 trials where we drew N trajectories with

replacement from each set of N trajectories, constructed a MSM with the drawn trajectories, and recomputed the observable of interest (e.g., MSM-weighted docking score). Refer to Table S2 for the number of trajectories and aggregate simulation data for each isoform.

IC50 to K_i Conversion

The mechanism by which blebbistatin inhibits skeletal muscle myosin's actin-activated ATPase activity has been characterized in detail[40]. These experiments indicate that blebbistatin binds with the highest affinity to myosin when it is in its ADP*Pi state capable of weakly binding to actin but also has non-negligible affinity for myosin in its ATP-bound state. Thus, blebbistatin can be considered a mixed inhibitor of actin-activated ATPase activity. The K_m for actin activation of S1 ATPase was 24 μM while the actin concentration used to determine blebbistatin's IC50 for skeletal muscle myosin was 43 μM[40]. Given that blebbistatin's affinity for the ADP*Pi state is 10x that of its affinity for the ATP-bound state and that $\frac{K_m}{S} = 0.56$, we conclude that IC50 is essentially equal to K_i for skeletal muscle myosin[75]. We assume that the same mechanism of inhibition applies to the other myosin-II isoforms and that IC50s for other myosin-II isoforms can be directly converted to K_i's. Thus, we pooled reported IC50s with K_i's across experiments and converted to binding free energies under these assumptions.

Code Availability

The code used for the generation, analysis, and visualization of the molecular dynamics data is available via a Github repository at https://github.com/bowman-lab/blebbistatin-specificity.

Acknowledgements

We would like to acknowledge the Folding@home community for its support and generous donation of computing resources. We would like to thank AMD for the donation of critical hardware and support resources from its HPC Fund that enabled many of the computations for this work. We would also like to thank Oracle Cloud Infrastructure for its donation of computational resources. AM was supported by the National Institutes of Health F30 Fellowship (1F30HL162431-01A1). JML was supported by the National Science Foundation (DGE2139839). This work was funded by NSF CAREER Award MCB-1552471 and NIH grants R01 GM124007 and RF1AG067194. G.R.B holds a Packard Fellowship for Science and Engineering from The David & Lucile Packard Foundation. This work was also supported by the National Institutes of Health (R01 HL141086 to M.J.G. and GM 20909 to L.A.L.) and the Children's Discovery Institute of Washington University and St. Louis Children's Hospital (PM-LI-2019-829 M.J.G.).

References

1. Longo, L. M. *et al.* On the emergence of p-loop ntpase and rossmann enzymes from a beta-alpha-beta ancestral fragment. *Elife* **9**, 1–16 (2020).
2. Knoverek, C. R., Amarasinghe, G. K. & Bowman, G. R. Advanced Methods for Accessing Protein Shape-Shifting Present New Therapeutic Opportunities. *Trends in Biochemical Sciences* (2019). doi:10.1016/j.tibs.2018.11.007
3. Wenthur, C. J., Gentry, P. R., Mathews, T. P. & Lindsley, C. W. Drugs for Allosteric Sites on Receptors. *http://dx.doi.org/10.1146/annurev-pharmtox-010611-134525* **54**, 165–184 (2014).
4. Dror, R. O. *et al.* Structural basis for modulation of a G-protein-coupled receptor by allosteric drugs. *Nature* **503**, 295–299 (2013).
5. Trivedi, D. V., Nag, S., Spudich, A., Ruppel, K. M. & Spudich, J. A. The Myosin Family of Mechanoenzymes: From Mechanisms to Therapeutic Approaches. *Annu. Rev. Biochem.* **89**, 667–693 (2020).
6. Wu, P., Clausen, M. H. & Nielsen, T. E. Allosteric small-molecule kinase inhibitors. *Pharmacol. Ther.* **156**, 59–68 (2015).
7. Hart, K. M. *et al.* Designing small molecules to target cryptic pockets yields both positive and negative allosteric modulators. *PLoS One* **12**, e0178678 (2017).
8. Cimermancic, P. *et al.* CryptoSite: Expanding the Druggable Proteome by Characterization and Prediction of Cryptic Binding Sites. *J. Mol. Biol.* **428**, 709–719 (2016).
9. Vajda, S., Beglov, D., Wakefield, A. E., Egbert, M. & Whitty, A. Cryptic binding sites on proteins: definition, detection, and druggability. *Curr. Opin. Chem. Biol.* **44**, 1–8 (2018).
10. Preller, M. & Manstein, D. J. 4.8 Myosin Motors: Structural Aspects and Functionality. in *Comprehensive Biophysics* 118–150 (Elsevier, 2012). doi:10.1016/B978-0-12-374920-8.00410-0
11. Teerlink, J. R. *et al.* Cardiac Myosin Activation with Omecamtiv Mecarbil in Systolic Heart Failure. *N. Engl. J. Med.* **384**, 105–116 (2021).
12. Olivotto, I. *et al.* Mavacamten for treatment of symptomatic obstructive hypertrophic cardiomyopathy (EXPLORER-HCM): a randomised, double-blind, placebo-controlled, phase 3 trial. *Lancet* **396**, 759–769 (2020).
13. FDA approves new drug to improve heart function in adults with rare heart condition | FDA. Available at: https://www.fda.gov/drugs/news-events-human-drugs/fda-approves-new-drug-improve-heart-function-adults-rare-heart-condition. (Accessed: 29th August 2022)
14. Barrick, S. K. & Greenberg, M. J. Cardiac myosin contraction and mechanotransduction in health and disease. *J. Biol. Chem.* **297**, (2021).
15. Tajsharghi, H. & Oldfors, A. Myosinopathies: pathology and mechanisms. *Acta Neuropathol.* **125**, 3 (2013).
16. Crucial role of myosin X in aggressiveness and metastasis. *Nat. Rev. Clin. Oncol.* **11**, 441–441 (2014).
17. Robert-Paganin, J. *et al.* Plasmodium myosin A drives parasite invasion by an atypical force generating mechanism. *Nat. Commun.* **10**, 1–12 (2019).
18. Preller, M. & Manstein, D. J. Myosin Structure, Allostery, and Mechano-Chemistry. *Structure* **21**, 1911–1922 (2013).

19. Robert-Paganin, J., Pylypenko, O., Kikuti, C., Sweeney, H. L. & Houdusse, A. Force Generation by Myosin Motors: A Structural Perspective. *Chem. Rev.* **120**, 5–35 (2020).
20. Bond, L. M., Tumbarello, D. A., Kendrick-Jones, J. & Buss, F. Small-molecule inhibitors of myosin proteins. *Future Med. Chem.* **5**, 41–52 (2013).
21. Straight, A. F. *et al.* Dissecting temporal and spatial control of cytokinesis with a myosin II inhibitor. *Science (80-.).* **299**, 1743–1747 (2003).
22. Limouze, J., Straight, A. F., Mitchison, T. & Sellers, J. R. Specificity of blebbistatin, an inhibitor of myosin II. *J. Muscle Res. Cell Motil.* **25**, 337–341 (2004).
23. Allingham, J. S., Smith, R. & Rayment, I. The structural basis of blebbistatin inhibition and specificity for myosin II. *Nat. Struct. Mol. Biol.* **12**, 378–379 (2005).
24. Rauscher, A., Gyimesi, M., Kovács, M. & Málnási-Csizmadia, A. Targeting Myosin by Blebbistatin Derivatives: Optimization and Pharmacological Potential. *Trends in Biochemical Sciences* **43**, 700–713 (2018).
25. Eddinger, T. J. *et al.* Potent Inhibition of Arterial Smooth Muscle Tonic Contractions by the Selective Myosin II Inhibitor, Blebbistatin. *J. Pharmacol. Exp. Ther.* **320**, 865–870 (2007).
26. Hong, H. W. *et al.* Blebbistatin inhibits the chemotaxis of vascular smooth muscle cells by disrupting the myosin II-actin interaction. *Am. J. Physiol. - Hear. Circ. Physiol.* **294**, 2060–2068 (2008).
27. Zhang, H. M. *et al.* Characterization of Blebbistatin Inhibition of Smooth Muscle Myosin and Nonmuscle Myosin-2. *Biochemistry* **56**, 4235–4243 (2017).
28. Várkuti, B. H. *et al.* A highly soluble, non-phototoxic, non-fluorescent blebbistatin derivative. *Sci. Reports 2016 61* **6**, 1–10 (2016).
29. Radnai, L. *et al.* Discovery of Selective Inhibitors forIn VitroandIn VivoInterrogation of Skeletal Myosin II. *ACS Chem. Biol.* **16**, 2164–2173 (2021).
30. Zimmerman, M. I. *et al.* SARS-CoV-2 simulations go exascale to predict dramatic spike opening and cryptic pockets across the proteome. *Nat. Chem.* 1–9 (2021). doi:10.1038/s41557-021-00707-0
31. Kuzmanic, A., Bowman, G. R., Juarez-Jimenez, J., Michel, J. & Gervasio, F. L. Investigating Cryptic Binding Sites by Molecular Dynamics Simulations. *Acc. Chem. Res.* (2020). doi:10.1021/ACS.ACCOUNTS.9B00613
32. Bowman, G. R., Bolin, E. R., Hart, K. M., Maguire, B. C. & Marqusee, S. Discovery of multiple hidden allosteric sites by combining Markov state models and experiments. *Proc. Natl. Acad. Sci. U. S. A.* **112**, 2734–2739 (2015).
33. Porter, J. R. *et al.* Cooperative Changes in Solvent Exposure Identify Cryptic Pockets, Switches, and Allosteric Coupling. *Biophys. J.* **116**, 818–830 (2019).
34. Hollingsworth, S. A. *et al.* Cryptic pocket formation underlies allosteric modulator selectivity at muscarinic GPCRs. *Nat. Commun.* **10**, 1–9 (2019).
35. Hendlich, M., Rippmann, F. & Barnickel, G. LIGSITE: Automatic and efficient detection of potential small molecule-binding sites in proteins. *J. Mol. Graph. Model.* **15**, 359–363 (1997).
36. Porter, J. R., Meller, A., Zimmerman, M. I., Greenberg, M. J. & Bowman, G. R. Conformational distributions of isolated myosin motor domains encode their mechanochemical properties. *Elife* **9**, (2020).
37. Muretta, J. M., Rohde, J. A., Johnsrud, D. O., Cornea, S. & Thomas, D. D. Direct real-time detection of the structural and biochemical events in the myosin power stroke. *Proc.*

Natl. Acad. Sci. **112**, 14272–14277 (2015).
38. Radnai, L. *et al.* Discovery of Selective Inhibitors forIn VitroandIn VivoInterrogation of Skeletal Myosin II. *ACS Chem. Biol.* **16**, 2164–2173 (2021).
39. *An Introduction to Markov State Models and Their Application to Long Timescale Molecular Simulation*. **797**, (Springer Netherlands, 2014).
40. Kovács, M., Tóth, J., Hetényi, C., Málnási-Csizmadia, A. & Seller, J. R. Mechanism of Blebbistatin Inhibition of Myosin II. *J. Biol. Chem.* **279**, 35557–35563 (2004).
41. Robert-Paganin, J., Auguin, D. & Houdusse, A. Hypertrophic cardiomyopathy disease results from disparate impairments of cardiac myosin function and auto-inhibition. *Nat. Commun.* **9**, 4019 (2018).
42. Ramamurthy, B., Yengo, C. M., Straight, A. F., Mitchison, T. J. & Sweeney, H. L. Kinetic mechanism of blebbistatin inhibition of nonmuscle myosin IIB. *Biochemistry* **43**, 14832–14839 (2004).
43. Hart, K. M., Ho, C. M. W., Dutta, S., Gross, M. L. & Bowman, G. R. Modelling proteins' hidden conformations to predict antibiotic resistance. *Nat. Commun.* **7**, 12965 (2016).
44. Sirigu, S. *et al.* Highly selective inhibition of myosin motors provides the basis of potential therapeutic application. *Proc. Natl. Acad. Sci. U. S. A.* **113**, E7448–E7455 (2016).
45. Snoberger, A. *et al.* Myosin with hypertrophic cardiac mutation r712l has a decreased working stroke which is rescued by omecamtiv mecarbil. *Elife* **10**, 1–24 (2021).
46. Greenberg, M. J. & Tardiff, J. C. Complexity in genetic cardiomyopathies and new approaches for mechanism-based precision medicine. *Journal of General Physiology* **153**, (2021).
47. Waterhouse, A. *et al.* SWISS-MODEL: homology modelling of protein structures and complexes. *Nucleic Acids Res.* **46**, W296–W303 (2018).
48. Abraham, M. J. *et al.* Gromacs: High performance molecular simulations through multi-level parallelism from laptops to supercomputers. *SoftwareX* **1**–**2**, 19–25 (2015).
49. Huang, J. *et al.* CHARMM36m: an improved force field for folded and intrinsically disordered proteins. *Nat. Methods 2016 141* **14**, 71–73 (2016).
50. Jorgensen, W. L., Chandrasekhar, J., Madura, J. D., Impey, R. W. & Klein, M. L. Comparison of simple potential functions for simulating liquid water. *J. Chem. Phys.* **79**, 926–935 (1983).
51. Bussi, G., Donadio, D. & Parrinello, M. Canonical sampling through velocity rescaling. *J. Chem. Phys.* **126**, 014101 (2007).
52. Parrinello, M. & Rahman, A. Polymorphic transitions in single crystals: A new molecular dynamics method. *J. Appl. Phys.* **52**, 7182 (1998).
53. Hess, B., Bekker, H., Berendsen, H. J. C. & Fraaije, J. G. E. M. LINCS: A Linear Constraint Solver for Molecular Simulations. *J Comput Chem* **18**, 14631472 (1997).
54. Shirts, M. & Pande, V. S. COMPUTING: Screen Savers of the World Unite! *Science* **290**, 1903–4 (2000).
55. Pérez-Hernández, G., Paul, F., Giorgino, T., De Fabritiis, G. & Noé, F. Identification of slow molecular order parameters for Markov model construction. *J. Chem. Phys.* **139**, 015102 (2013).
56. McGibbon, R. T. & Pande, V. S. Variational cross-validation of slow dynamical modes in molecular kinetics. *J. Chem. Phys.* **142**, 124105 (2015).
57. Prinz, J.-H. *et al.* Markov models of molecular kinetics: Generation and validation. *J.*

Chem. Phys. **134**, 174105 (2011).
58. Wu, H. & Noé, F. Variational approach for learning Markov processes from time series data. *J. Nonlinear Sci.* **30**, 23–66 (2017).
59. Pande, V. S., Beauchamp, K. & Bowman, G. R. Everything you wanted to know about Markov State Models but were afraid to ask. *Methods* **52**, 99–105 (2010).
60. Scherer, M. K. *et al.* PyEMMA 2: A Software Package for Estimation, Validation, and Analysis of Markov Models. *J. Chem. Theory Comput.* **11**, 5525–5542 (2015).
61. Porter, J. R., Zimmerman, M. I. & Bowman, G. R. Enspara: Modeling molecular ensembles with scalable data structures and parallel computing. *J. Chem. Phys.* **150**, (2019).
62. Trott, O. & Olson, A. J. AutoDock Vina: Improving the speed and accuracy of docking with a new scoring function, efficient optimization, and multithreading. *J. Comput. Chem.* **31**, 455–461 (2010).
63. Koes, D. R., Baumgartner, M. P. & Camacho, C. J. Lessons learned in empirical scoring with smina from the CSAR 2011 benchmarking exercise. *J. Chem. Inf. Model.* **53**, 1893–1904 (2013).
64. Grossfield, A., Feller, S. E. & Pitman, M. C. Convergence of molecular dynamics simulations of membrane proteins. *Proteins Struct. Funct. Bioinforma.* **67**, 31–40 (2007).
65. Romo, T. D. & Grossfield, A. LOOS: an extensible platform for the structural analysis of simulations. *Annu. Int. Conf. IEEE Eng. Med. Biol. Soc. IEEE Eng. Med. Biol. Soc. Annu. Int. Conf.* **2009**, 2332–2335 (2009).
66. Romo, T. D., Leioatts, N. & Grossfield, A. Lightweight Object Oriented Structure analysis: Tools for building Tools to Analyze Molecular Dynamics Simulations. *J. Comput. Chem.* **35**, 2305 (2014).
67. Coelho, L. P. Jug: Software for Parallel Reproducible Computation in Python. *J. Open Res. Softw.* **5**, 30 (2017).
68. GNU Parallel: The Command-Line Power Tool | USENIX. Available at: https://www.usenix.org/publications/login/february-2011-volume-36-number-1/gnu-parallel-command-line-power-tool. (Accessed: 5th September 2022)
69. Resnicow, D. I., Deacon, J. C., Warrick, H. M., Spudich, J. A. & Leinwand, L. A. Functional diversity among a family of human skeletal muscle myosin motors. *Proc. Natl. Acad. Sci. U. S. A.* **107**, 1053–1058 (2010).
70. Sommese, R. F. *et al.* Molecular consequences of the R453C hypertrophic cardiomyopathy mutation on human β-cardiac myosin motor function. *Proc. Natl. Acad. Sci. U. S. A.* **110**, 12607–12 (2013).
71. Deacon, J. C., Bloemink, M. J., Rezavandi, H., Geeves, M. A. & Leinwand, L. A. Identification of functional differences between recombinant human α and β cardiac myosin motors. *Cell. Mol. Life Sci.* **69**, 2261–2277 (2012).
72. Clippinger, S. R. *et al.* Disrupted mechanobiology links the molecular and cellular phenotypes in familial dilated cardiomyopathy. *Proc. Natl. Acad. Sci. U. S. A.* **116**, 17831–17840 (2019).
73. Greenberg, M. J., Shuman, H. & Ostap, E. M. Inherent Force-Dependent Properties of β-Cardiac Myosin Contribute to the Force-Velocity Relationship of Cardiac Muscle. *Biophys. J.* **107**, L41–L44 (2014).
74. De, E. M., Cruz, L. & Ostap, E. M. Chapter 6 - Kinetic and Equilibrium Analysis of the Myosin ATPase. doi:10.1016/S0076-6879(08)04206-7

75. Yung-Chi, C. & Prusoff, W. H. Relationship between the inhibition constant (KI) and the concentration of inhibitor which causes 50 per cent inhibition (I50) of an enzymatic reaction. *Biochem. Pharmacol.* **22**, 3099–3108 (1973).
76. Planelles-Herrero, V. J., Hartman, J. J., Robert-Paganin, J., Malik, F. I. & Houdusse, A. Mechanistic and structural basis for activation of cardiac myosin force production by omecamtiv mecarbil. *Nat. Commun.* **8**, 190 (2017).
77. Dominguez, R., Freyzon, Y., Trybus, K. M. & Cohen, C. Crystal Structure of a Vertebrate Smooth Muscle Myosin Motor Domain and Its Complex with the Essential Light Chain: Visualization of the Pre–Power Stroke State. *Cell* **94**, 559–571 (1998).
78. Ropars, V. *et al.* The myosin X motor is optimized for movement on actin bundles. *Nat. Commun. 2016 71* **7**, 1–13 (2016).

Figures and Tables

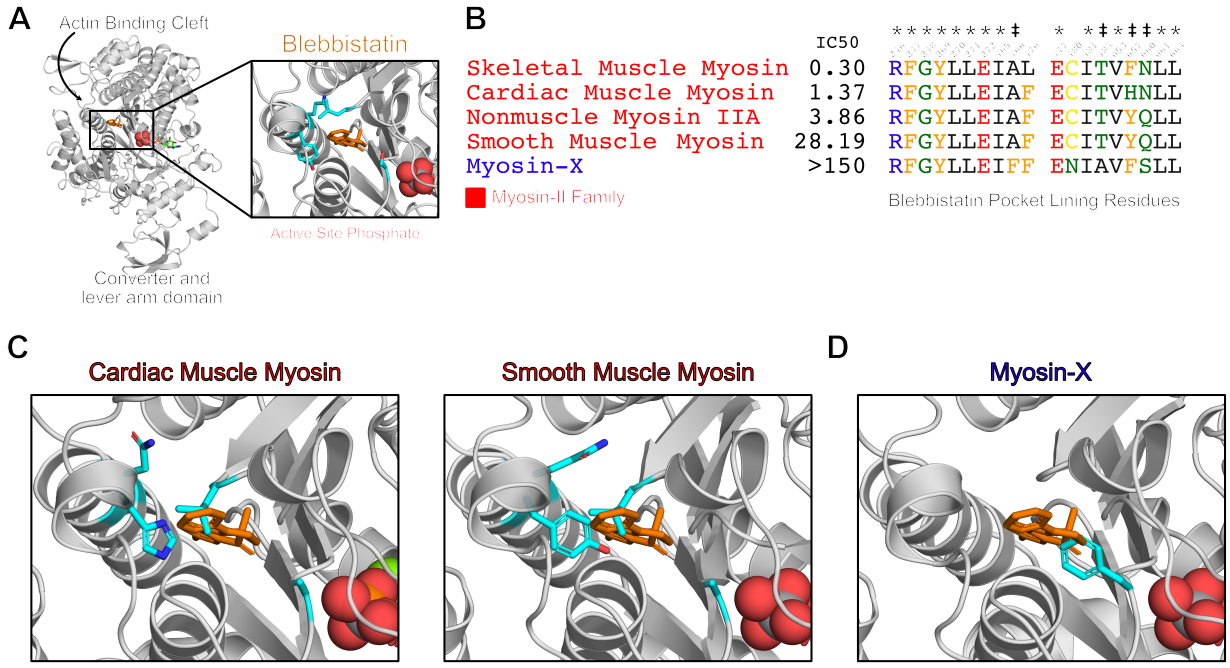

Figure 1. Blebbistatin's cryptic binding pocket is closed in blebbistatin-free experimental myosin structures and the sequence of surrounding residues is highly conserved across myosin isoforms with widely varying IC50s. A. The motor domain of a *D.d.* myosin-II molecule bound to blebbistatin. The inset depicts blebbistatin's cryptic binding pocket (PDB: 1YV3[23]). Blebbistatin is shown in orange sticks while the active site phosphate is shown in spheres. Select residues (same as those shown in C) are shown in their *holo* position in cyan sticks. **B.** Alignment of blebbistatin contact residues (within 5 Å of blebbistatin in 1YV3) reveals that 16 of 19 residues are identical among myosin-IIs despite almost two orders of magnitude difference in blebbistatin IC50. We also include an unconventional myosin-X to highlight an important sequence difference at residue 466 (A vs. F) that separates blebbistatin-sensitive (IC50 < 150 μM) and blebbistatin-insensitive isoforms (IC50 > 150 μM). A star indicates a residue is conserved among all myosin isoforms shown. A double cross is used to indicate sequence differences previously suggested to play an important role in determining blebbistatin specificity[23]. **C.** Crystal structures of β-cardiac (PDB: 5N6A[76]) and smooth muscle myosin (1BR2[77]) do not suggest an obvious mechanism for differences in blebbistatin potency between these isoforms. In both structures, the cryptic blebbistatin-binding pocket is closed, and an aligned blebbistatin molecule (orange) clashes with a leucine residue (cyan). The two residues that differ between these isoforms (cyan histidine and asparagine in cardiac; cyan tyrosine and glutamine in smooth) do not form specific interactions with blebbistatin (e.g., hydrogen bonds). **D.** In a blebbistatin-free myosin-X structure (PDB: 5I0H[78]), F436 (cyan) forms a large steric impediment to blebbistatin binding (aligned molecule shown in orange) that is not present in myosin-II isoforms.

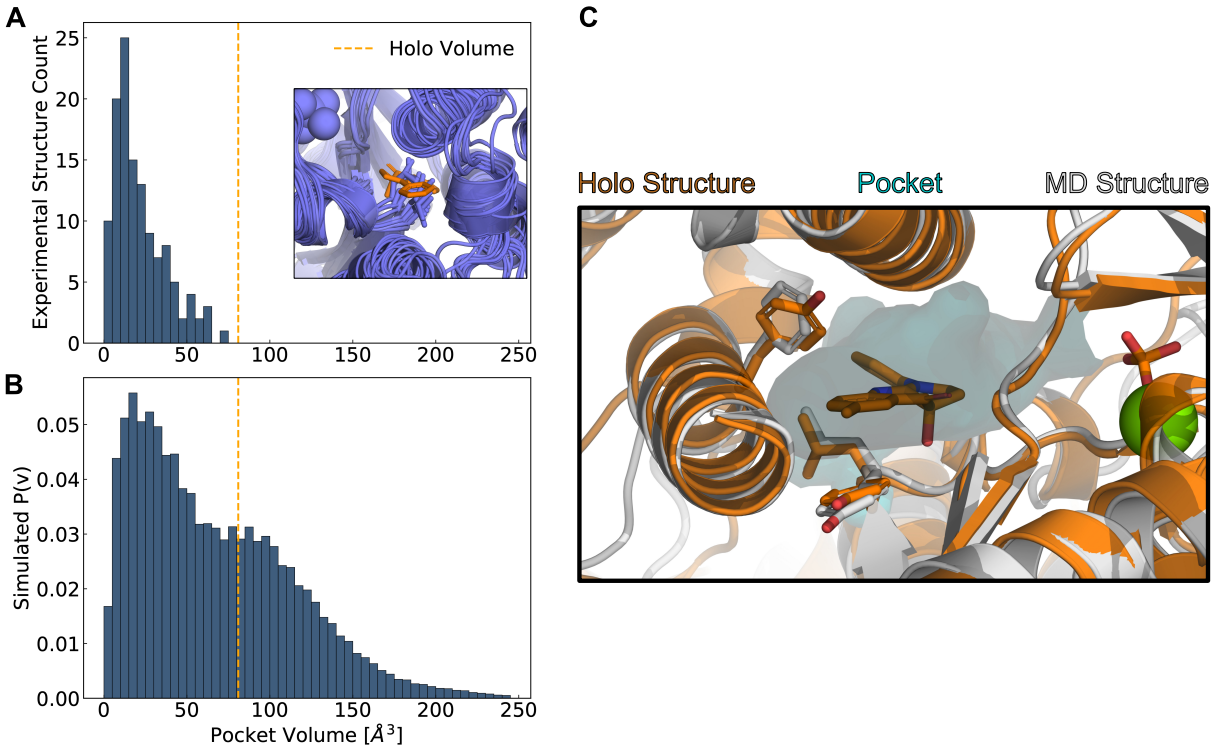

Figure 2. Simulations reveal opening of blebbistatin's cryptic pocket. **A.** The distribution of pocket volumes from experimental crystal structures queried from the Protein Data Bank shows that the blebbistatin pocket is cryptic. The inset is a random selection of 15 structures from the accompanying distribution with an overlaid blebbistatin molecule in orange. All experimentally determined myosin structures display steric clash with a blebbistatin molecule aligned based on its contact residues in a *holo* structure (PDB: 1YV3). **B.** Blebbistatin pocket volumes in simulations of fast skeletal myosin IIA reveal substantial pocket opening. The blebbistatin pocket volume from a ligand-bound crystal structure (PDB: 1YV3) is delineated by an orange vertical line in both panels. Simulated P(v) corresponds to the probability of adopting a given volume for each bin in the histogram. **C.** MD simulations explore open *holo*-like states. Structure of an open conformation of the blebbistatin binding pocket from MD simulations reveals good structural alignment with the *holo* crystal structure (0.55 Å root mean square deviation of contact residue backbone heavy atom and Cβ positions). Blebbistatin is shown in cyan with the pocket from the MD structure shown as a cyan contour. Select residues in the blebbistatin pocket (Y269, L270, and F657) have the same backbone and sidechain positions as in the *holo* crystal structure.

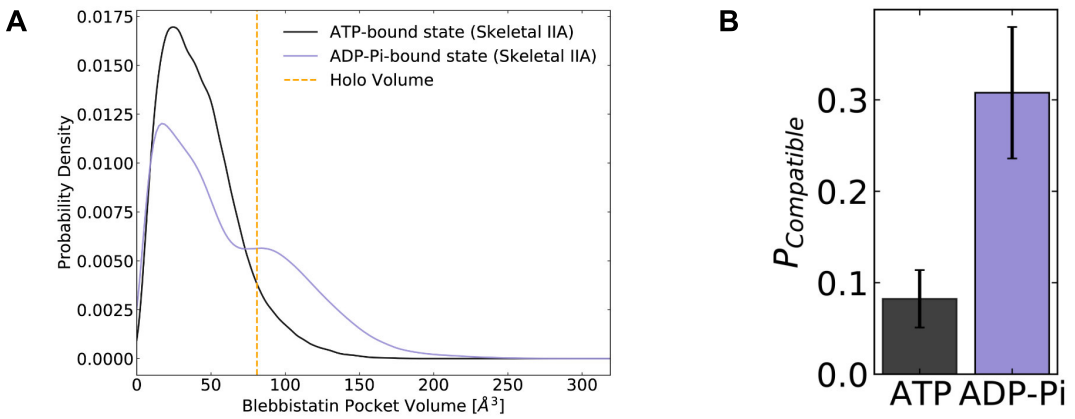

Figure 3. Blebbistatin pocket opening preferentially occurs in the ADP*Pi state. A. Distributions of skeletal muscle myosin IIA blebbistatin pocket volumes in the ATP-bound state and ADP*Pi-bound state demonstrate that the blebbistatin pocket is more likely to open in the ADP*Pi-bound state, consistent with biochemical experiments which predict tighter binding between blebbistatin and myosin when myosin is bound to ADP*Pi. **B.** The probability of adopting compatible structures (i.e., structures with pocket volumes equal to or greater than the *holo* crystal structure) is higher when myosin is bound to ADP and phosphate. Error bars represent estimate of standard error of the mean from 250 trials of bootstrapping where trajectories were drawn with replacement from the entire dataset (see Methods).

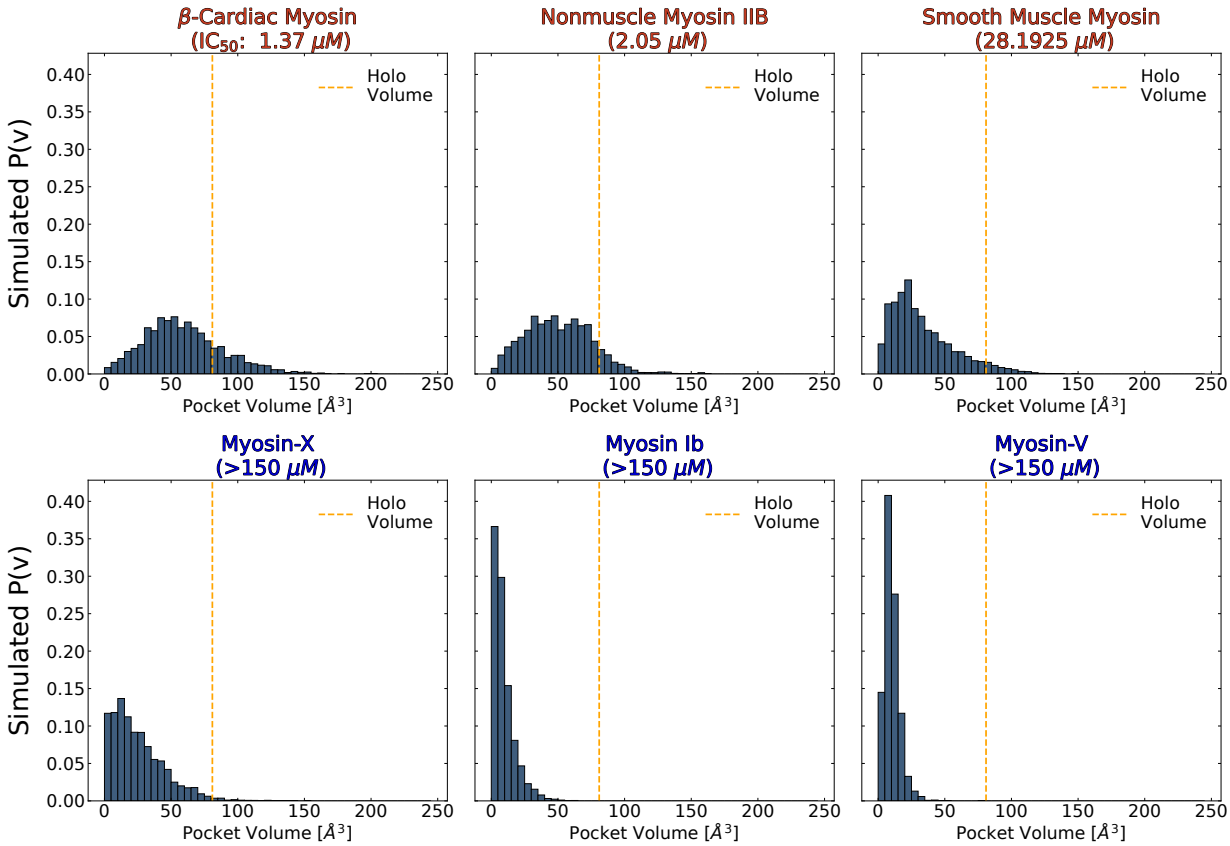

Figure 4. The probability of adopting open pocket conformations is greater among blebbistatin-sensitive isoforms (top row) than insensitive isoforms (bottom row). MSM-weighted distributions of blebbistatin pocket volumes in simulations of nucleotide-free isolated myosin motor domains show that myosin-IIs (top row) are more likely to exceed the blebbistatin pocket volume of a *holo* crystal structure (PDB: 1YV3, orange line) than non-class II myosins. Among myosin-IIs, those with lower IC50s[22,25–28,38] have more right-shifted pocket volume distributions.

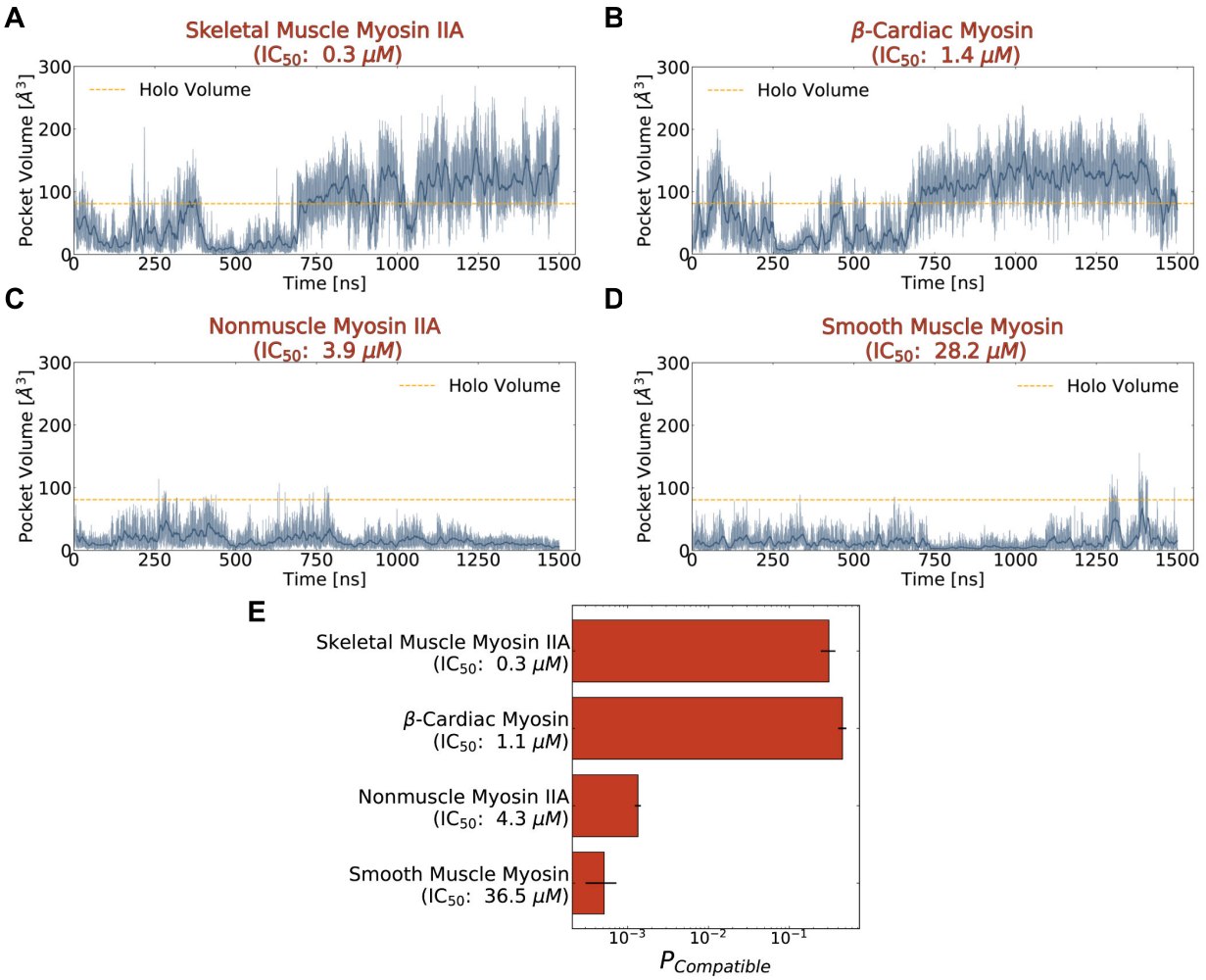

Figure 5. Blebbistatin cryptic pocket opening is more likely in simulations of highly sensitive myosin-II isoforms than in simulations of less sensitive myosin-IIs. A-D. Representative pocket volume trajectory traces for several myosin-II isoforms show that pocket opening occurs with greater frequency and that the pocket stays open for longer in those isoforms more potently inhibited by blebbistatin (top row). The dotted orange line delineates the blebbistatin pocket volume in a *holo* crystal structure (PDB ID: 1YV3). Transparent blue lines indicate raw data while the opaque blue lines are a 10 ns rolling average. **E.** Blebbistatin pocket opening is highly probable (>0.25) in skeletal muscle myosin II and β-cardiac myosin but highly unlikely (<0.01) for nonmuscle myosin IIA and smooth muscle myosin. A conformation was considered compatible if its blebbistatin pocket volume exceeded the pocket volume of a *holo* crystal structure (PDB ID: 1YV3). Conformations were weighted by their equilibrium probability in Markov State Models of the blebbistatin pocket. Error bars show bootstrapped estimate of standard error of the mean from 250 trials.

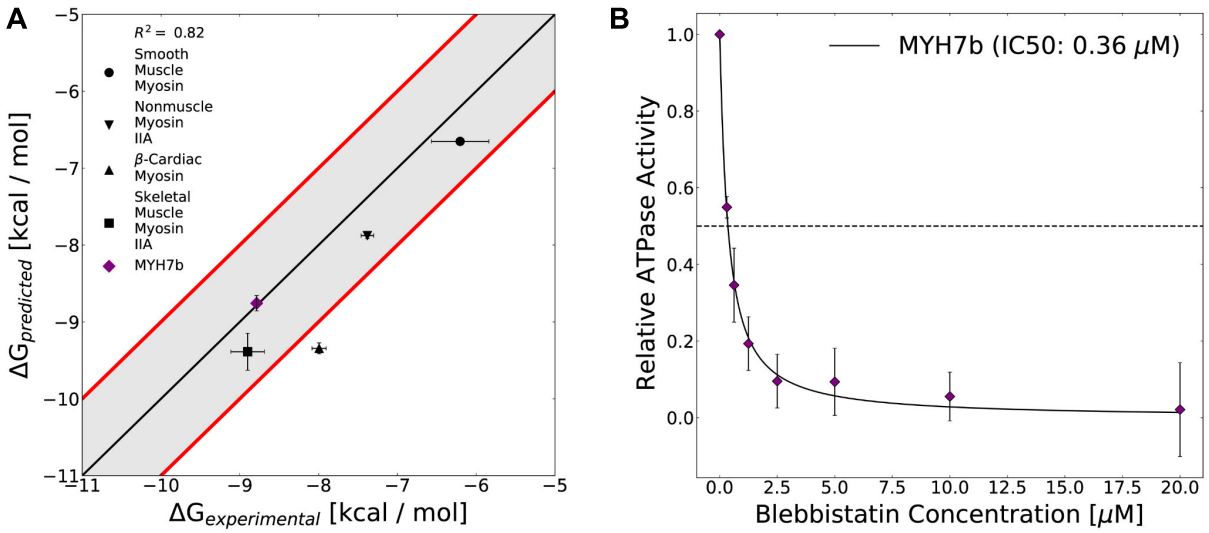

Figure 6. The computed free energy of binding for blebbistatin from MSM-docking accurately predicts binding free energies for existing experimental data and for a myosin isoform whose blebbistatin sensitivity was not known. A. Predictions from MSM-docking are highly correlated to experimental values ($R^2 = 0.82$) and most predictions are within 1 kcal/mol of experimental values. Error bars for predicted free energies of binding represent bootstrapped estimate of standard error of the mean from 250 trials. Error bars for experimental values show the standard error of the IC50 or K_i converted to a binding free energy. **B.** An NADH-linked ATPase assay indicates that MYH7b is highly sensitive to blebbistatin inhibition (IC50: 0.36 μM), consistent with the prediction from MSM-docking. Data show the mean ATPase activity ± standard deviation across 5 experimental replicates.